

---

---

# Optimization of Water and Nitrate Use Efficiencies for Almonds Under Micro Irrigation

---

---

**Project No.:** 14-PREC4-Hopmans

**Project Leader:** Jan W Hopmans  
Department of Land, and, Air and Water Resources  
UC Davis  
One Shields Ave.  
Davis, CA 95616  
530.752.3060  
jwhopmans@ucdavis.edu

**Project Cooperators and Personnel:**

Maziar M. Kandelous and Valentin Couvreur, Department of LAWR,  
UC Davis  
Patrick Brown, Department of Plant Science, UC Davis  
Blake Sanden, Farm Advisor, UCCE - Kern County

## 1. Objectives:

This field study provides critical information on the movement of water and nutrients through the soil under variable soil moisture conditions, and provides insight into the interactions of applied irrigation water and nitrogen fertilizer, soil physical properties, soil layering and crop root growth with nutrient use efficiency, minimizing losses of water (leaching and evaporation) and nitrogen (leaching and denitrification).

The final goal of this research project is to field-validate, optimize and refine the HYDRUS model under a variety of fertigation regimes using the on-going nutrient study in almonds implemented by P. Brown et al. Results will be used to optimize the management of irrigation and fertigation in an almond orchard. The specific objectives of this project are:

- a) To determine optimal irrigation and fertigation practices for micro-irrigation (drip and micro-sprinkler) systems for almond, to improve water and nutrient use efficiencies, and to reduce leaching and gaseous losses of nitrates, using a wide range of possible management scenarios (water, fertigation, salinity);
- b) To evaluate the results using the HYDRUS model from extensive field data for specific treatments, and refine it if so needed.

The objectives are achieved by collecting relevant field data such as soil hydraulic and textural properties with soil layering, monitoring of soil moisture and soil water potential, soil temperature and nitrate solution concentration for selected treatments, in addition to data already being collected as part of the larger nutrient management project. The data collection and analysis is very important, since all future model calibration and validation will be based on these data. A final optimization model will provide best management practices for various relevant micro-irrigation layouts with corresponding optimum irrigation and fertigation scheduling for a range of soil types.

## 2. Interpretive Summary:

Micro-irrigation methods have proven to be highly effective in achieving the desired crop yields, but there is increasing evidence suggesting the need for the optimization of irrigation scheduling and management, thereby achieving sustainable agricultural practices, while minimizing losses of applied water and nutrients at the field scale.

To optimize irrigation/fertigation of almonds, it is essential that irrigation and fertilizers are applied at the optimal concentration, place, and time to ensure maximum root uptake. Moreover, sound and sustainable irrigation systems must maintain a long-term salt balance that minimizes both salinity impacts on crop production and salt leaching to the groundwater. The applied irrigation water and dissolved fertilizer, as well as root growth and associated nutrient and water uptake, interact with soil properties and fertilizer source(s) in a complex manner that cannot easily be resolved with 'experience' and field experimentation alone. It is therefore that state-of-the-art modeling is required with the field observations, to allow for unraveling of the most obvious complexities as a result of the typical wide spatial variations of soil texture and layering across farmer-managed fields.

The goal of this research project is to optimize management practices for various micro-irrigation systems for almond, minimizing losses of water (leaching and evaporation), nitrogen (leaching and denitrification), and crop yields by water and salinity stress (droughts). In addition, the applied HYDRUS model with associated root water and nutrient uptake will be evaluated using extensive datasets as acquired from an ongoing nutrient management field project. Therefore, the research project consists of two main components: (a) determining the optimal irrigation and fertigation practices for micro-irrigation (drip and micro-sprinkler) systems for almond, to improve water and nutrient use efficiencies, and to reduce leaching and gaseous losses of fertilizer Nitrogen, using a wide range of possible management scenarios (water, fertigation, salinity), and (b) evaluation of the results using the HYDRUS model from extensive field data for specific treatments, and to refine it if needed.

To achieve this goal, this project emphasizes the collection of relevant field data such as soil hydraulic properties, soil texture, and soil layering, and continued monitoring of soil moisture, soil water potential, temperature, salinity, and soil solution nitrate concentration for selected irrigation type treatments. For each of the two irrigation treatments, soil profiles were analyzed to identify soil layers with corresponding textural and hydraulic properties. An extensive set of ECHO-TE soil moisture sensors (Decagon, Inc.), tensiometers, and soil water solution samplers were installed in the tree root zone to monitor the spatial and temporal changes of soil water content, total soil water potential, soil salinity, temperature, and soil solution nitrate. A special tensiometer was designed to monitor and estimate leaching rates of applied irrigation water and nitrate fertilizers.

The 2014-15 annual report focuses on (a) the analysis of variation on applied water, soil water storage, and heterogeneity in soil textural and hydraulic properties at both tree plot and field scales, and (b) the inverse modeling (HYDRUS) approach to estimate leaching of water as well as hydraulic properties of different layers within and below the root zone. The ultimate goal of this analysis is to assess and evaluate leaching rates of water and nitrate fertilizer throughout the year for both irrigation treatments. In general, much of leaching amounts and

rates are largely controlled by irrigation type, soil layering, and applied water (irrigation and precipitation) relative to evapotranspiration (ET). The combined installation of tensiometers with solution samplers below the rooting zone are the best way to measure leaching rate of both water and nitrate. Although their operating range is limited to relatively wet soils, this is not a limitation for our purpose as leaching is only relevant if the soil is wet. The main limitation is caused by the large uncertainty of the soil's unsaturated hydraulic conductivity. We recommend using existing databases such as Neuro Multistep as applied in this study, and/or to using in-situ soil moisture and soil matric potential data to infer soil hydraulic properties by inverse modeling. It is shown that the deep soil profile in this study is fairly dry toward the maximum tensiometer range, suggesting negligible leaching of water and consequently nitrate under common irrigation/fertigation management practices of the past three years.

Alternatively, we propose to apply a tree-scale and field-scale water balance technique using spatially-distributed soil moisture measurements to infer leaching rate and its spatial variations as caused by soil heterogeneity, and variation in applied water. We show that the water balance approach may lead to considerable leaching uncertainty unless all the components of the water balance equation are available at the same scale and their associated uncertainties are low. Tentatively, our data suggest that water and nitrate losses in our study area are low, because of the 3-year drought as caused by associated low winter/spring precipitation.

This past year, we focused on focus on water balance simulations using HYDRUS, and to conduct a sensitivity analysis procedure that allows extrapolation of specific field outcome to other soil types. We also noticed the effect of local ET on the outcome of inverse modeling and used down-scaling techniques to estimate tree scale ET using field scale ET and locally monitored parameters such as soil water storage, mid-day stem water potential, and PAR.

### **3. Materials and Methods:**

The presented methods were used for an almond orchard consisting of two micro-irrigation systems, drip and fanjet. A total of 40 trees across the field were monitored in which 20 trees were located in drip block, and 20 trees in fanjet block. For each irrigation system (block), one tree was selected for detailed instrumentation for the purpose of real-time monitoring of soil-water and tree status. The study is part of an ongoing project at Wonderful Orchards in Lost Hills (near Bakersfield). A schematic of the location of monitored trees in the field, fanjet and drip block, and two heavily instrumented trees is presented in **Figure 1**.

#### **3.1. Soil characterization**

Among the most important information is an evaluation of the presence of soil layers, and the textural/hydraulic properties of each individual layer for typical soil profiles. Using the layering information obtained from soil cores in 2011, we took six undisturbed soil samples (8-cm diameter by 6-cm tall) around each of the heavily instrumented trees (one in fanjet, one in drip) to measure the hydraulic properties of deep soil profile (Two depths of 190, and 210 cm each with three replicates). The constant head method along with pressure cell (Tempe Cell) experiment was used to measure the soil water retention curves, saturated hydraulic conductivity, and unsaturated hydraulic conductivity functions for each layer. The soil hydraulic properties are required to (1) estimate soil water storage and retention, and (2) compute leaching rate from the unsaturated hydraulic conductivity using Darcy's equation (Eq. [1]).

Also, the bulk density, porosity, saturated water content, and the soil texture of each individual core was determined. As it became clear early on that the variability of soil texture and layering was large, we collected a total of 160 additional soil samples to a soil depth of 2.5 m at both tree scale treatments. From these, the majority of soil samples (110 samples) were undisturbed samples (both using manual core sampler and hydraulic giddings), from which either soil bulk density and/or saturated hydraulic conductivity were measured. Rather than measuring the unsaturated hydraulic properties for each soil sample (which is time consuming and complicated), we used the neural network approach by Budiman et al. (2004). Based on past soil hydraulic measurements from SJV soils, this so-called Neuro Multistep method allows for prediction of soil hydraulic properties using more easily to obtain soil properties of soil texture, soil bulk density and saturated hydraulic conductivity. These soil samples, however, were taken to evaluate the variability of soil physical and hydraulic properties, and layering at tree scale. Therefore, to evaluate the field scale heterogeneity and variability in layering, a total of 360 additional undisturbed soil samples (one sample at each 30-cm depth interval down to 2.7 m, from each of the 40 monitored trees) were collected and analyzed to obtain the field mean and variation of bulk soil density, porosity, and soil texture.

### **3.2. Soil monitoring**

#### **3.2.1. Soil moisture and soil water potential**

Unfortunately, many of ECHO-5TE (Decagon Inc.) soil moisture sensors installed by PureSense in 2011 were useless, because of malfunctioning of sensors and data collection issues. Therefore, we installed a new set-up in 2012. A total of 30 ECHO-5TE (Decagon Inc.) soil moisture sensors were installed in the rooting zone of each of the two tree locations in a grid pattern (**Figure 2**), thereby instrumenting one quarter of the tree's rooting zone, at depths of 30, 60, 90, 120 and 150 cm for 6 spatial locations (**Figure 3**). An additional set of sensors were installed at the same depths below the berm in the fanjet plot along the center line (Y-direction) (**Figure 3**). The sensor installation grid was designed such that measurements provide soil information halfway between trees (Y direction), and up to the distance influenced by wetting pattern of either fanjet or drip perpendicular to the trees row (in X direction).

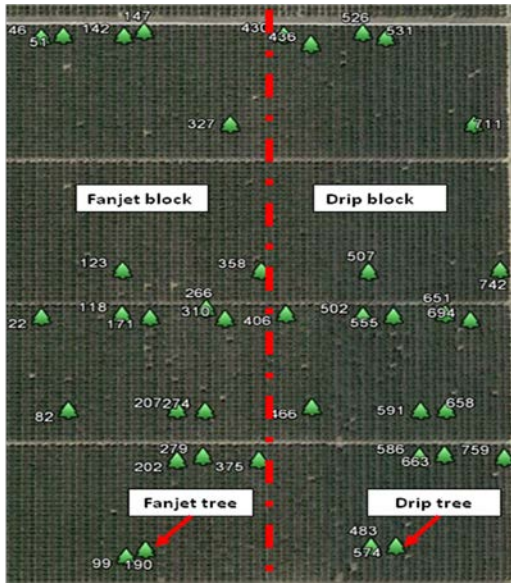


**Figure 1.** Locations of monitored trees in almond orchard (field), two irrigation systems (Fanjet and Drip block), and the two heavily instrumented trees (Fanjet and Drip tree).

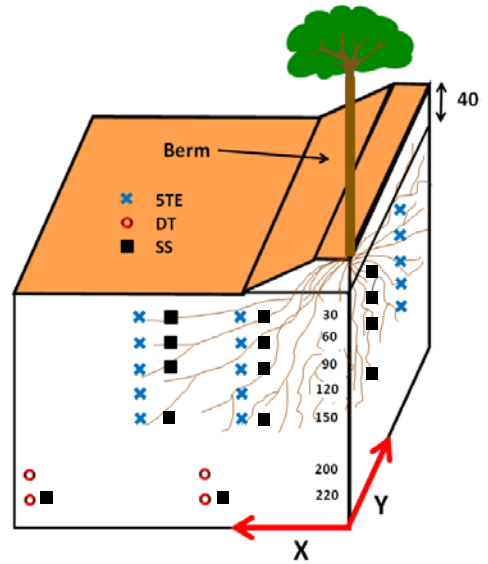


**Figure 2.** A schematic showing installation depths of various sensor types, with 5TE representing the ECHO-5TE soil moisture, DT the deep tensiometers, and SS referring to soil solution samplers.

The ECHO-5TE provides for measurement of volumetric soil water content, as well as for soil salinity (Electrical Conductivity or EC), and soil temperature. For the purpose of installation, holes were dug with a 5" hand auger. Sensors were provided and are being monitored by PureSense Environmental Inc.

Four pairs of deep tensiometers (red circles) were installed at both fanjet and drip irrigation sites to monitor the total head gradient below the root zone. Two pairs of tensiometers were installed below the canopy where the irrigation water is applied representing the wet part below the root zone and the other two pairs were placed at the middle distance between two tree rows, representing the most dry region for both treatments.

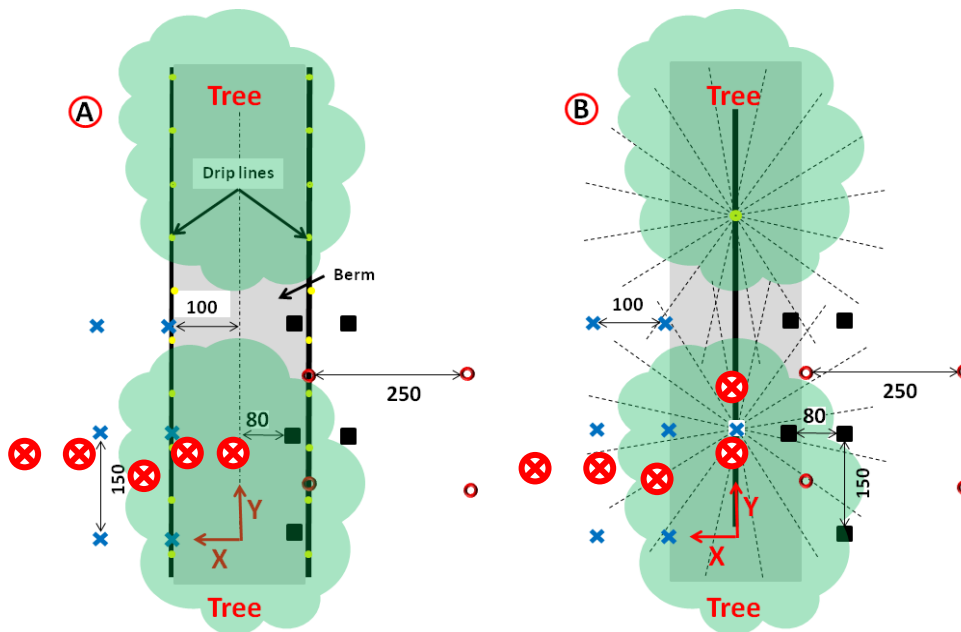


**Figure 3.** A schematic top view of the installed soil moisture sensors, deep tensiometers, and solution samplers in (A) Drip and (B) Fanjet site. The red crossed circles denote the approximate location for the neutron probe access tubes.

In addition, five neutron probe access tubes were installed in neighboring tree plots (**Figure 3**) for each treatment, allowing for soil moisture and soil water storage measurements to a depth of 2.7 m in 30-cm depth intervals. In addition to the two 5-probe instrumented (called hereafter heavily instrumented) trees, a total of 38 trees were instrumented with a single access tube in order to monitor the soil water storage at the field scale. The location of the single access tube relative to its nearby tree trunk was the same for each instrumented tree across the field, and corresponded to the location of the third access tube for the heavily instrumented trees. Most of the neutron probe measurements were collected approximately one day prior to each irrigation event. The neutron probe was calibrated using independent gravimetric soil moisture samples using linear regression, with a non-zero intercept (See **Figure 4A**). We note that the soil water storage estimated using a single access tube is not as representative for the tree-scale as determined from instrumented trees using 5 neutron access tubes. Therefore, for each of the two heavily instrumented trees, the measured soil profile water storage using the 5-tube setup was correlated to the water storage using only the main access tube across the field (**Figures 4 B and C**), and this correlation was subsequently applied to single-access-tube monitored trees (**Figure 3**), for computation of the field-scale water balance.

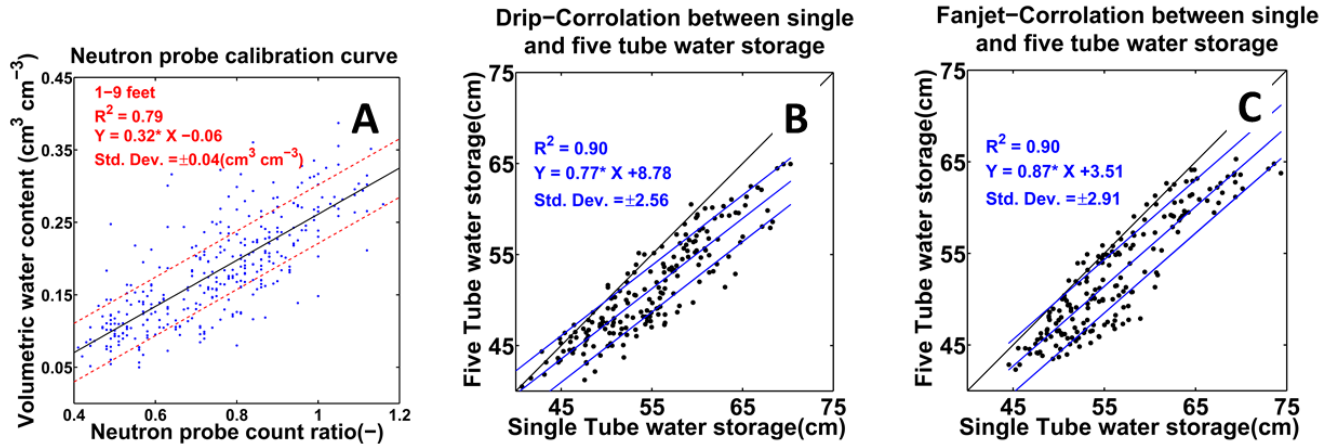


**Figure 4. A:** Neutron probe calibration curves with blue circles representing samples from entire orchard **B:** Correlation between soil water storage using single probe and 5-probes setup in fanjet tree. **C:** Correlation between soil water storage using single probe and 5-probes setup in drip tree.

### 3.2.2. Leaching rate calculations

Leaching rates can be estimated if the hydraulic conductivity and the total head gradient across the soil layer below the root zone are known. The leaching flow rate,  $q_{AB}$ , can be calculated using the Darcy equation as follows:

$$q_{AB} = -K(h) \frac{H_B - H_A}{\Delta z_{A-B}} \text{ or } q_{AB} = -K(\theta) \frac{H_B - H_A}{\Delta z_{A-B}}, \quad (1)$$

where  $q$  denotes the Darcy water flux (inches day<sup>-1</sup>),  $K(h)$  or  $K(\theta)$  represent the unsaturated soil hydraulic conductivity, which is a function of the soil matric potential  $h$  or  $\theta$  at the deep measurement depth. In the Darcy equation,  $H_A$  and  $H_B$  denote the total water head values at bottom and top of the soil layer below the root zone, respectively, and  $\Delta z_{A-B}$  signifies the thickness of the soil layer between the tensiometers. As shown in **Figure 2** the set of deep tensiometers were installed at four different locations at depths of 200 and 220 cm. Using the measured soil matric potential values above and below the impeding layer and its thickness, we computed the total head gradient for each of four individual measurement locations for each site. Using the measured soil water matric potentials and soil water content along with the unsaturated hydraulic conductivity for the soil layer in question, one calculates the leaching rates by multiplying the unsaturated hydraulic conductivity with the total head gradient, according to Eq. [1]. The choice of using either water content or pressure head measurements for the conductivity estimation depends on the accuracy of the measurement and the sensitivity of either of the two variables on the unsaturated hydraulic conductivity value (see section 4.1). We used the hydraulic conductivity based on soil matric potential,  $K(h)$ , as we concluded that the measured soil matric potential measurements with the deep tensiometers were very accurate in the wet soil moisture range.

### 3.3. Additional required input data for modeling

In addition to soil physical characterization, other required input data for the HYDRUS modeling includes measurements of tree evapotranspiration (ET), water application rates, and

spatial distribution for the drip and fanjet systems, fertigation amounts and rates, and tree root distribution. Daily ET rates were available from eddy-covariance data collected at the fanjet site, whereas volumetric flow rates were determined from flow meter measurements installed in the irrigation lines.



**Figure 5.** Measurement (a and b) of water application uniformity and uniformity pattern (c) for the fanjet (1 hour volume measurements).

The wetted area for the drip system is monitored by visual inspection, whereas the water application uniformity of the fanjet system was determined from measurement of water volumes in 110 10-cm diameter catch cans, distributed within the quarter section of the instrumented fan jet plot (**Figure 5**). Though additional uniformity data was collected, soil moisture patterns indicate that the measured patterns are consistent during the irrigation season.

### 3.4. Water balance

In addition to estimation of leaching rates using the Darcy equation from tensiometric measurements (Eq. 1), leaching rates (L) can be determined from the tree-scale and field-scale water balance, using measurements of applied irrigation water (IW), precipitation (P), tree evapotranspiration (ET), and changes in soil water storage ( $\Delta S$ ) to a specific soil depth below the rooting zone. As the depth of the soil water storage measurements increased, we expect the estimated L to be more accurate, as it would increasingly account for upward capillary rise, if relevant. Thus, from periodic measurements of  $\Delta S$ , and corresponding data of IW (flow meter measurements), P (CIMIS station #146), ET (eddy covariance tower) and  $\Delta S$  (neutron probe), the leaching rate (L) can be computed from:

$$L = IW + P - ET - \Delta S \quad , (2)$$

with the measurement unit expressed in depth of water (cm). The water balance was computed between irrigation events across the 2009-2013 monitoring seasons. Whereas IW, P, and ET are area-wide measurements, we divided the heavily instrumented tree plot in two equal size sections, representing the tree rooting zone (along the tree rows) and dry zone (section between tree rows), where  $\Delta S$  from the dry zone was determined from the neutron probe measurements furthest away from the tree row. The amount of water applied through irrigation system (IW) was monitored from flow meters for each site. The water volume delivered to each tree was divided to the area occupied by each tree yielding the equivalent depth of applied irrigation water. The number of dripper (20 drippers of 4 l/hr per tree) designed was such that the amount water delivered to each tree was equal to the amount of



water applied to each tree of the fanjet site (2 fanjets of 40 l/hr per tree).

#### 4. Results and Discussion:

##### 4.1. Soil textural analysis

Analysis of soil texture for both the fanjet and drip trees showed that the soil profile of the studied almond orchard is highly heterogeneous and layered. **Figure 6** shows representative soil layers and differences of soil profiles between the drip and fanjet tree. The top one meter of soil profile at the fanjet site consists of coarse soil material, allowing quick infiltration of applied irrigation water. The profile includes two 20 cm thick fine-textured soil layers at approximate depths of 130 and 200 cm soil depth.

We believe the difference in depths of clay layers between the two irrigation plots has significant implications on leaching rates. These layers will prevent and/or delay downward water movement below the root zone. The drip site shows depth variations in soil texture as well, with the fine-textured soil layer at about the 180 cm.

Fan Jet	Clay (%)	Silt (%)	Sand (%)	Depth (cm)	Sand (%)	Silt (%)	Clay (%)	Drip
Sandy clay loam	21	18	61	10	73	12	15	Sandy loam
				20				
				30				
	27	26	47	40	75	13	12	
				50				
				60				
	21	26	53	70	72	15	13	
Loam				80				Clay loam
				90				
	28	27	45	100	37	32	31	
Clay				110				loam
	54	27	19	130	43	38	19	
Sandy loam	19	25	56	140				Sandy clay loam
loam	23	32	45	170	48	27	25	
Sandy loam	14	12	74	180				Clay
				190	21	37	42	
Silt clay	44	47	6	200				Clay loam
				210				
Clay loam				220	37	29	34	Sandy loam
				230				
				240				
				250	62	19	19	
				260				
				270				

**Figure 6.** A schematic with soil layers and soil texture for the drip and fanjet sites.

Further soil core sampling at both experimental sites was needed to ascertain the depth variation of soil texture and hydraulic properties, and their spatial heterogeneity of soil profiles within and between the two irrigation sites. **Figure 7** present the spatial heterogeneity of soil properties and layering within and between Drip and Fanjet irrigation sites in both tree (heavily instrumented trees) and field (single-access-tube equipped trees) scale. Although there are significant variations in soil layering and textural/hydraulic properties, the soil layering at tree scale plots follow the same pattern as was identified at the beginning of this project (**Figure 5**). Also, there was consistency in the data, with depth variations in saturated hydraulic conductivity (Ksat), coinciding with either depth variations in soil bulk density or sand/clay content. For example, the clay and clay loam layers in **Figure 6** correspond with soil layers of decreasing Ksat for both the drip (100 and around 200 cm) and fanjet (100 and 180 cm) sites. Despite the huge variation in soil layering and textural properties at the field scale, our interpretation is that the field scale layering and depth variation in bulk density in each irrigation site corresponds somewhat with that determined from the single tree soil profiles. Specifically, the sand content is maximum at depths near 30 and 180 cm across the field for the fanjet treatment. For the drip site, both the tree and field scale plots show correspondence of coarse-textured soils in the top 100 cm soil profile.

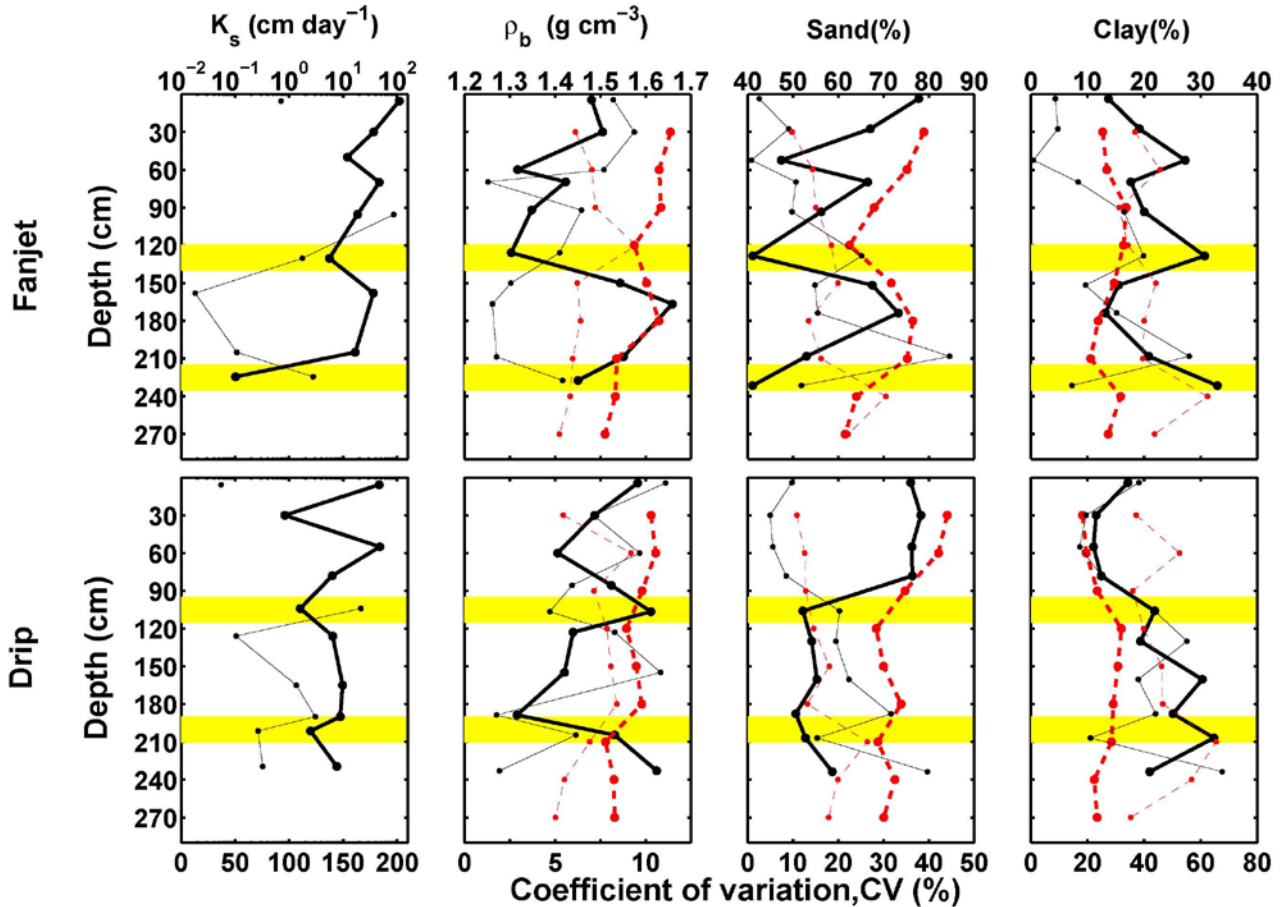


**Figure 7.** Mean (thick line) and CV (thin line) values of saturated hydraulic conductivity ( $K_{sat}$ ), dry bulk density, sand and clay content as a function of soil depth for tree (solid black line) and field (Dashed red line) scale. The yellow horizontal bars represented the location of fine textured soil layer.

#### 4.2. Soil hydraulic properties

**Figure 8** shows the soil water retention and unsaturated hydraulic conductivity curves for core samples from the deep soil profile at depths of 190 and 210 cm. In **Figures 8 A & B**, the soil water retention curve was measured using the Tempe cell method along with the constant head approach for saturated hydraulic conductivity. The results show the enormous variability of the soil water retention curves, thereby resulting in high uncertainty of the unsaturated hydraulic conductivity.

Though not shown in this report, we previously compared the Neuro Multistep predictions with measured hydraulic functions, and concluded that the predicted curves agreed fairly well with the measured ones. Hence, it was decided to apply the Neuro Multistep model to predict both the soil water retention and unsaturated hydraulic conductivity curves using the soil physical data from the collected 21 soil samples (12 samples from drip and 9 samples from fanjet site) of the 200-240 cm depth interval for both tree plots. The results are also presented in **Figures 8 C & D**. From the curves in **Figures 8 C & D**, it becomes instantly clear that the variation in soil water retention and unsaturated hydraulic conductivity is enormously large, even when considering the 200-240 cm depth interval only. Hence, accurate information of soil textural

properties (both mean and variation) is extremely important to estimate leaching rates and its field-scale variations.

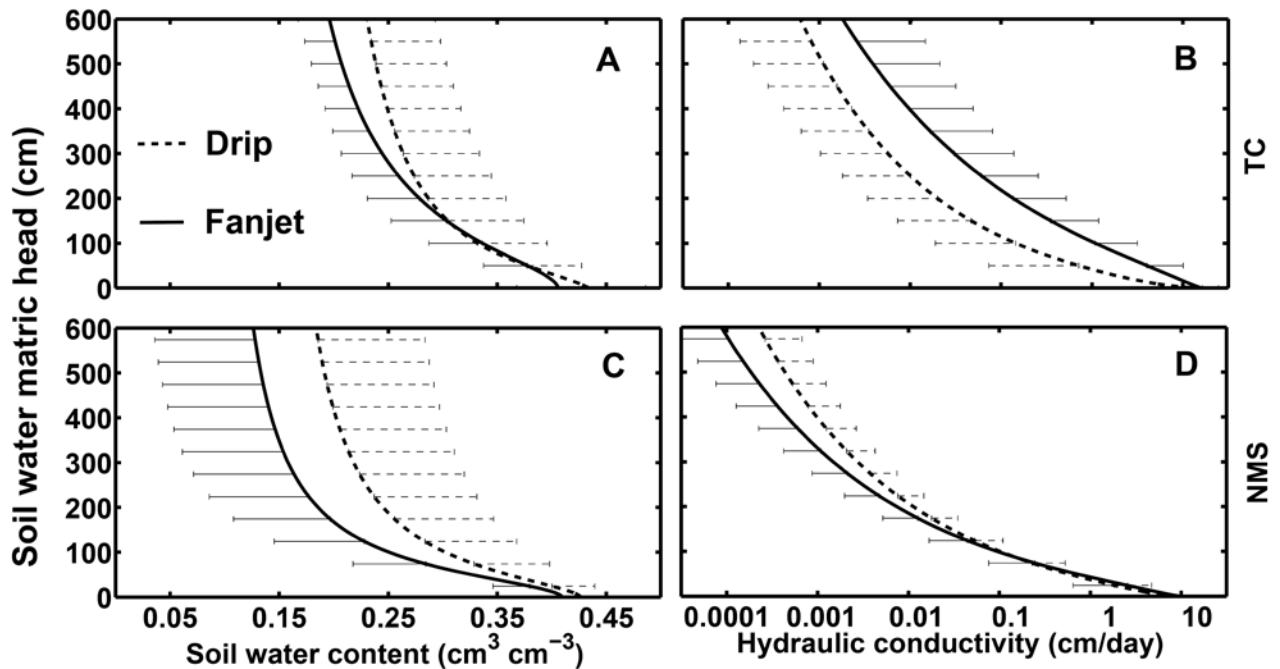


**Figure 8.** Soil water retention (left plots) and unsaturated hydraulic conductivity (right plots) curves for the different soil types in drip (dashed line) and fanjet (solid line) sites. The error bars represent the standard deviation.

#### 4.3. Leaching rate

The amount of water leaching ( $L$ , cm) for both irrigation sites was analyzed using two different approaches. The first method uses the water balance at two scales of tree plot and field, from measurements of applied water, evapotranspiration, and soil water storage measurements (section 4.3.1). In the second approach, we applied Darcy equation [1], to compute leaching rates from tensiometric soil water potential measurements, and measured soil hydraulic properties along with predicted unsaturated hydraulic conductivity values using the Neuro Multistep method (section 4.3.2). The presented water balance was computed for the 2009-2013 period.

##### 4.3.1. Water balance<sup>1</sup>

*Precipitation ( $P$ ) and Evapotranspiration ( $ET$ )*

**Figure 9** shows the monthly precipitation and evapotranspiration of the water balance equation. The precipitation data come from a nearby CIMIS station (#146) and was assumed representative for the whole field (both drip and fanjet treatments), so that precipitation rates were the same for the water balance, irrespective of scale (irrigation block or tree plot). The amount of precipitation in the first two years (late fall 2009 and 2010 and early winter 2010 and 2011) was significantly higher as compared with the last two years.

<sup>1</sup> Collaboration with Blake Sanden, farm advisor in Kern County, UC Extension Center.

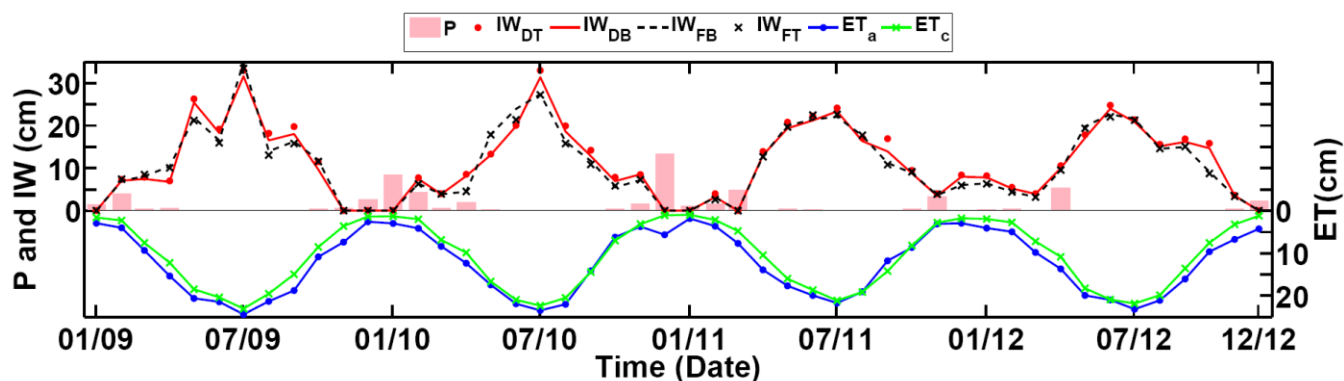


**Figure 9.** Monthly evapotranspiration, ET, and applied irrigation water, IW, and precipitation, P. The applied water, IW, for DT, DB, FB, and FT, respectively are shown by red circle, red solid line, dashed black line, and black cross. Pink bar plot shows precipitation. In right y-axis, potential evapotranspiration, ET<sub>p</sub>, is shown by cross-marked green line, while actual evapotranspiration, ET<sub>a</sub>, is presented by circle-marked blue line.

Depends on the soil profile water storage during the rainy season, the precipitation water may be stored in the soil profile or leave the rooting zone as deep percolation if the soil water content exceed the field capacity. The right y-axis show the monthly potential and actual evapotranspiration obtained from CIMIS station and Eddy-Covariance tower located in the orchard for four consequence years. Similar to the precipitation data, we assumed that ET rates were identical, irrespective of scale. Comparing the precipitation and evapotranspiration data presented in **Table 1**, it is shown that the amount of precipitation is about 10% of evapotranspirative demand indicating the irrigation dependency of the agricultural practice in the studied area.

**Table1.** A summary of the water balance components for field, irrigation block, and tree scale for the 2009-13 monitoring period.

	P (cm)	ET <sub>a</sub> (cm)	IW (cm)	ΔS (cm)	L (cm)
	57.7	580	mean (± std)		
DB			545.8 (±20.4)	0 (±5.5)	23.5 (±20.4)
FB			527.8 (±15.1)	2.3 (±4.8)	2.9 (±16.3)
DT			572.7 (±3.3)	1.5 (±1.6)	48.7 (±4.8)
FT			509.6 (±3.1)	9 (±1.6)	-21.8 (±4.7)

#### Applied irrigation water (IW)

**Figure 9** shows also the monthly applied water for four consecutive years of the 2009 – 2013 for both drip and fanjet in irrigation block and tree plot scale. In contrast to the precipitation and evapotranspiration which was assumed to be uniform across the field, the amount of applied irrigation water was determined locally using 30 flowmeters<sup>2</sup> installed across the field (15 in drip site, and 15 in fanjet site). **Table 1** show the cumulative amount of applied water at tree and irrigation block scale for both drip and fanjet sites. The origin of variation presented in **Table 1** is from two sources of a) the uncertainty associated with flowmeter reading, and b) the variation in applied irrigation water between different locations across the orchard. Our data show that there is ±7 % variation in IW across the orchard which corresponds to 72 cm (29

<sup>2</sup> There were initially total of 30 trees with flowmeters starting from 2009, but 10 trees were added in 2010. Hence, we used the initially 30 monitored trees to cover four years of 2009-2013.

inches for four years) difference between minimum and maximum applied water, indicating the non-uniformity associated within and between the two irrigation systems. **Figure 10** shows the location of flow meters installed across the field, in which the relative variation of IW is shown by circle size. It is shown that the average and variation in applied water in the drip site are higher than the fanjet site, suggesting either greater change in soil water storage, higher leaching, or higher ET for the drip site. However, in a field scale evaluation it is shown that the sum of field averaged IW and P data is equal to the  $ET_a$ , confirming a well-managed field with irrigation scheduling based on ET.

### Soil water storage ( $\Delta S$ )

The last component of the water balance equation, that is required for leaching calculations, is the change of soil water storage. We used the available neutron probe data, as these provided soil water content measurements down to 2.7 m.

**Figure 11** shows the cumulative changes in soil water storage for four consecutive years of the 2009 – 2013 for drip and fanjet sites in both tree plot and irrigation block scales. The soil water storage increases with winter precipitation when the crop water demand is the lowest, and it decreases during the growing season with losses due to ET or leaching. On an annual basis, it is shown that the overall soil water storage does not change. However, the soil water storage in fanjet tree increased from one year to another, and this is because of the initially dryer soil water profile at the fanjet tree at the beginning of this study on 2009. The uncertainties presented in irrigation block scales are considerable and originated from three sources:

a) the uncertainty in Neutron Probe calibration curve presented in **Figure 4-A**; b) the uncertainty in transformation curves from one- to five- access tubes (**Figures 4-B and C**); and c) the variation between different locations across the orchard (**Figure 10**). However, the uncertainty presented in tree plot scale is less than those shown in irrigation block scale data, since it only carries the uncertainty in Neutron Probe calibration curve.

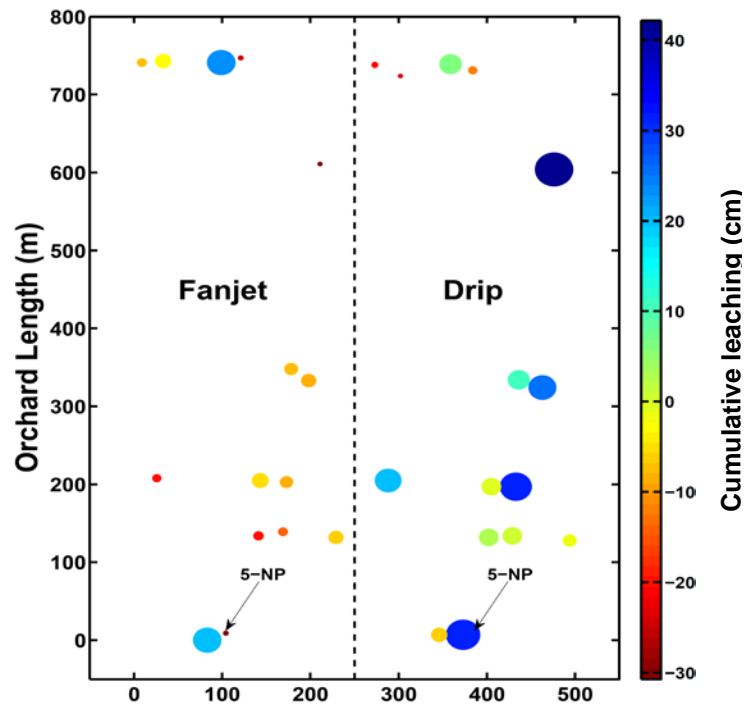


**Figure 10.** Locally measured Irrigation Water (IW) (circle size) and leaching (color bar) across the orchard. The minimum and maximum amount of total IW is 492 and 564 cm, respectively.

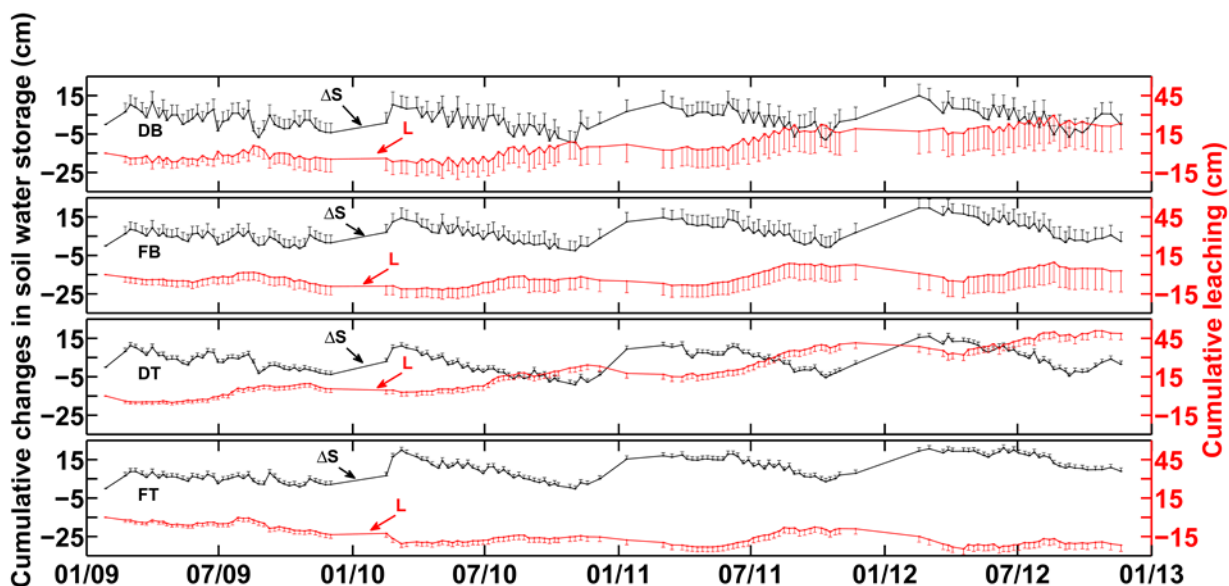


**Figure 11.** Cumulative amount of in soil water storage (black line), and leaching (red line) in DT, DB, FB, and FT for four consecutive of years of 2009-2013. Average values are presented by the thick lines, whereas the spatial variations are presented by the error bars, defined by standard deviations.

### *Leaching (L)*

The amount water lost through leaching can be calculated using the water balance equation (Eq. 2), since all other components are known.

**Figure 11** presents the calculated cumulative leaching for four consecutive years of the 2009 – 2013 for drip and fanjet sites in both tree plot and irrigation block scales. The uncertainty shown in these figures are mainly introduced by the uncertainty associated with applied irrigation water. It is also shown in **Figure 10** that locations with high leaching (color bar) correspond to the locations with high amount of applied water (size of the circle). A summary of the water balance components is presented in **Table 1**. With prior knowledge that the orchard was irrigated based on the ET and depletion of soil water storage, the field average leaching plot confirms a well-managed irrigation scheduling with minimum average leaching (almost zero). The applied water in drip block (DB) was higher than ET-P ( $IW > ET-P$ ), while it was smaller for the fanjet block, resulting in estimated leaching values of 23.5 cm for the drip block, and of about 2.9 cm for the fanjet block. We note here that all of the calculations were made with the assumption of uniform evapotranspiration (ET) across the orchard. It is known that plants adjust their water demand based on water availability, suggesting that trees with higher applied water transpire higher than the field average ET, and vice versa. The applied irrigation water in drip tree was about 60 cm higher than the fanjet, resulting in a difference of 70 cm in leaching between the drip and fanjet tree plots. The higher value in leaching difference is related to differences in changes in soil water storage (1.5 cm for drip vs. 9.1 cm for fanjet).

#### 4.3.2. Darcy equation

Leaching rates were computed from the Darcy Eq. [1], considering the uncertainty in (a) soil water matric potential measurements, (b) unsaturated hydraulic conductivity curves, and (c) soil texture of the soil layers at the deep tensiometer locations. Therefore, rather than calculating single leaching rate values, we computed leaching rate uncertainty in addition. However, since the tensiometers were installed in the spring of 2012, we only report values starting May, 2012. The deep soil profile was very dry and as a result the soil matric potential was out of the tensiometry range. We therefore stopped maintaining the deep tensiometers at the end of summer 2013 since the soil profile stayed dry due to the extreme drought condition with almost no meaningful precipitation followed by ~50% reduction in applied water in 2014.

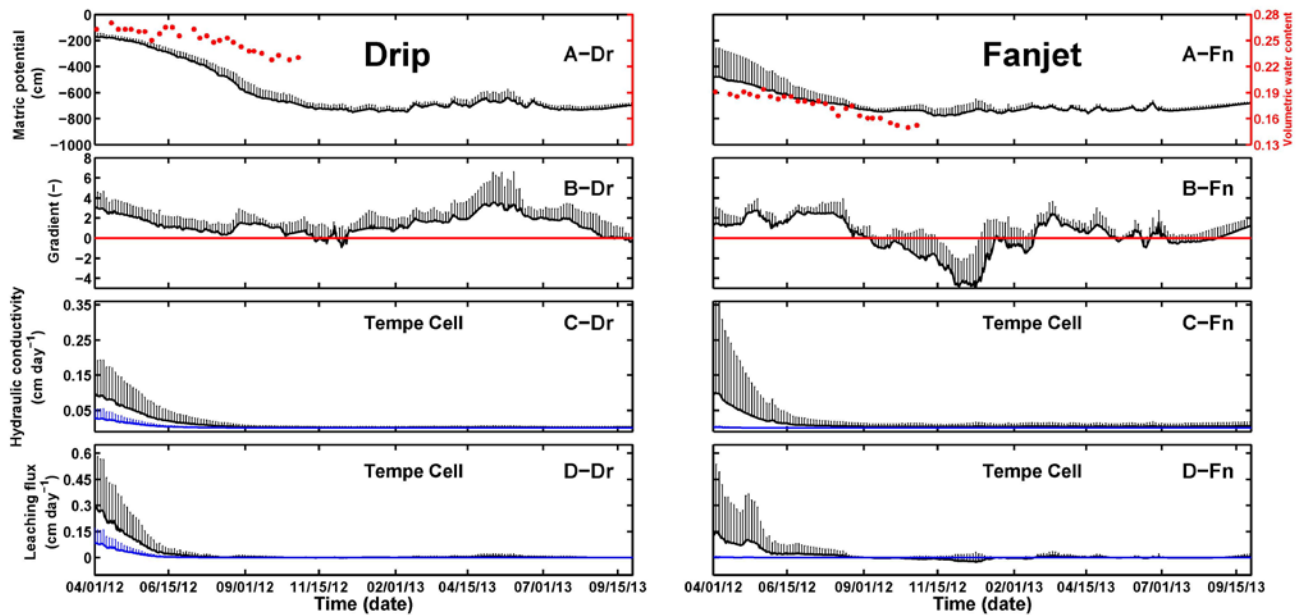


**Figure 12.** Spatial and temporal variations of (A) matric potential at the 200 and 220 cm soil depth, (B) total head gradient, (C) unsaturated hydraulic conductivity for multistep (black lines) and Neuro Multistep (blue lines) methods, and (D) leaching rate for multistep (black lines) and Neuro Multistep (blue lines) methods, as measured for 4 locations (**Figure 1**), starting April 1, 2012 through Sep 30, 2013. Average values are presented by the thick lines, whereas the spatial variations are presented by the error bars, defined by standard deviations. Red circles show the soil water content measured at depth of 210 cm using neutron probe.

**Figure 12 A** presents the average and standard deviation of matric potential values measured at the 200 and 220 cm soil depths for the drip and fanjet trees, respectively. As a result of increasing root water uptake and crop transpiration from spring to summer, the matric potential of the soil layer below the root zone gradually decreases (more negative) for both trees, but does not increase during the winter due to very low winter rainfall. It is shown that the deep soil matric potential slightly increased over the 2012 irrigation season, but not enough to have meaningful effect on soil leaching. We note that the matric potential values of the drip site are much larger (less negative) than for the fanjet site, because of either the clay layer presence at the tensiometer depth or greater amount of applied irrigation water discussed in previous section, or both. Moreover, the drier soil at the fanjet site is caused by reduced hydraulic conductivity of the clay layer above the 120 cm soil depth. The much larger uncertainty of the matric head values at the fanjet location is likely caused by the nonuniformity of the water

application and reduced lateral spreading above the deep soil layers because of the lower water content at this site (panel B), as opposed to the drip site as caused by higher IW values.

From the measured matric head values at the 200 and 220 cm soil depths, the total head gradient with corresponding spatial variations (standard deviation values) are plotted in **Figure 12 B**. Typically, average total head gradients in fanjet site vary between 2 and 4, indicating downward soil water flow, but gradually decreasing through the summer and fall. However, the tensiometer usually starts to drain at suction of about -700 cm, which would correspond (accounting for tensiometer length ~ 200 cm in our case) to the soil matric potential of -500 cm. Therefore, the gradient obtained at soil matric potential of about -500 or more negative can be over- or underestimated. The same trend is shown for the drip. Variations are typically large, and are caused by uncertainty in tensiometer readings and soil heterogeneity.

In order to compute the leaching rate at the 200-220 cm soil depth, we need to substitute the unsaturated hydraulic conductivity value of this layer in Eq. [1], which is dependent on soil texture and soil water matric potential at the tensiometer locations. However, because of the large variations in both matric potential and soil texture, we present the range in unsaturated hydraulic conductivity (**Figure 12 C**) as determined from the uncertainty ranges of matric potential (**Figure 12 A**) and unsaturated hydraulic conductivity curves (**Figure 8**). The latter is controlled by soil texture, but is partly unknown because of the apparent high spatial variability of soil texture and soil layering. Therefore, for each tree we calculated the unsaturated hydraulic conductivity of six soil cores collected from two depths of 190 and 210 cm, each with three replications. The unsaturated hydraulic conductivity varies by order of magnitudes thereby playing as dominant factor in calculating the leaching by Darcy equation. Despite the lower matric potential (less negative) in drip compare to fanjet, the average and range of corresponding hydraulic conductivity are the same as the soil cores from fanjet represent a finer textured soil than those in drip. However, the variation in matric potential for the fanjet is large thereby resulting in larger variation in hydraulic conductivity in fanjet compare to drip. The final estimated leaching rate values are presented in **Figures 12 D**, with mean leaching rate values ranging between 0-0.3 ( $\pm 0.26$ ) cm/day for drip and 0-0.15 ( $\pm 0.35$ ) cm/day for the fanjet.

In addition to computing leaching rates from the measured unsaturated hydraulic conductivity curves, we include in **Figure 12 C**, the predicted hydraulic conductivity curves and associated uncertainty, using the Neuro Multistep results of **Figure 8**. As the results indicate, the predicted hydraulic conductivities (blue lines in panel C) are close to the measured values for drip. However, the majority of predicted hydraulic conductivities in fanjet falls into the coarse textured soil category resulting in very low conductivity at the ranges of matric potential measured in fanjet. Blue lines in **Figure 12 D** show the leaching rates calculated using the hydraulic conductivities estimated by the neural network model.

#### 4.3.3. Comparison of leaching between water balance and Darcy equation approaches

**Table 2** shows a comparison between the cumulative leaching estimated using the water balance and the Darcy equation approach, using both measured (Multi-step) and predicted (Neuro Multi-step) unsaturated hydraulic conductivity curves. We note that the estimated uncertainty is significantly larger for the Darcy calculations, but in general the total cumulative L values are reasonably close between the two methods.



**Table 2.** Comparison of L and uncertainty range from water balance and Darcy equation approaches.

	Water balance	Darcy-Multistep K(h)	Darcy-Neuro Multistep K(h)
<b>Leaching (cm)</b>			
Drip	18.7 ( $\pm 2.6$ )	11.6 ( $\pm 13.6$ )	3.7 ( $\pm 3.2$ )
Fanjet	1.4 ( $\pm 2.5$ )	6.3 ( $\pm 16$ )	0

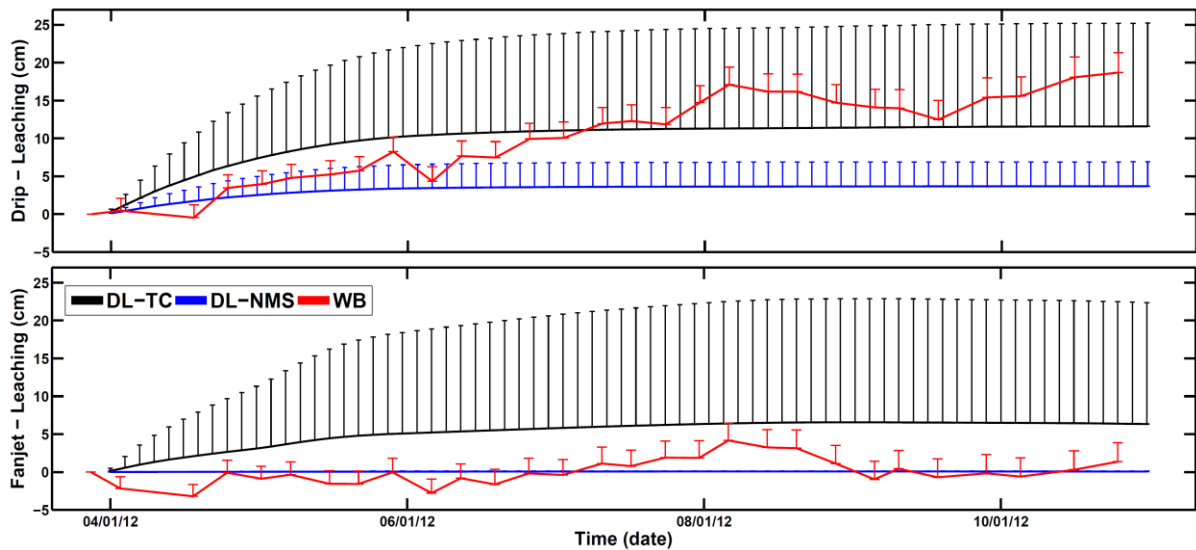


**Figure 13.** Comparison of leaching and the associated uncertainty range obtained from three different approaches of a) water balance (Red line), b) Darcy equation with measured soil hydraulic properties with combination of constant head and tempe cell (black line), and c) Darcy equation with predicated soil hydraulic properties using NeuroMultistep model (blue line).

**Figure 13** presents the calculated cumulative leaching using the above mentioned three approaches. The large uncertainty comes from the heterogeneity in soil properties and the corresponding high uncertainty of the soil hydraulic conductivity of the layer below the root zone. Evaluating the uncertainty range presented for drip and fanjet, one could conclude that the main uncertainty came from unsaturated conductivity, especially in the wet end, because L values tend to be near zero in the dry water content range. The uncertainty presented for the mass balance approach is small, because we used a uniform ET along with a small uncertainty for both locations. However, additional uncertainty of leaching rates from the mass balance approach is caused by unknown spatial variations of local ET and P across the field. We propose that inverse modeling, using HYDRUS and in-situ soil moisture and water potential data will provide a better and more certain approach for estimation of soil hydraulic properties in the future.

4.3.4. Inverse modeling approach to estimate the hydraulic conductivity and leaching  
 As was suggested in section (4.3.3), we implemented the inverse modeling (HYDRUS) approach to find the best fit between simulated and measured soil water content, thereby estimating the hydraulic properties of different layers, especially of the instrumented layer, to

estimate the leaching of water below the root zone using Darcy approach. **Figure 14** shows the simulated ET, leaching, as well as observed and simulated soil water content at different depths in fanjet tree (FT). The red circles show soil water content measured by neutron probe at different depths (d) from 30 to 270 cm in 30 cm intervals. Black lines show the average of simulated soil water content in 16 different scenarios with error bars representing their standard deviation. Despite of very small difference between simulated and observed soil water content, the variations presented in simulated evapotranspiration and leaching are fairly large. It is shown that the unknown local ET, introduces a large uncertainty (CV = 12%) in simulated (inversely estimated) local ET which has a direct effect on simulated leaching, thereby introducing a large uncertainty (CV = 46%) in simulated leaching.

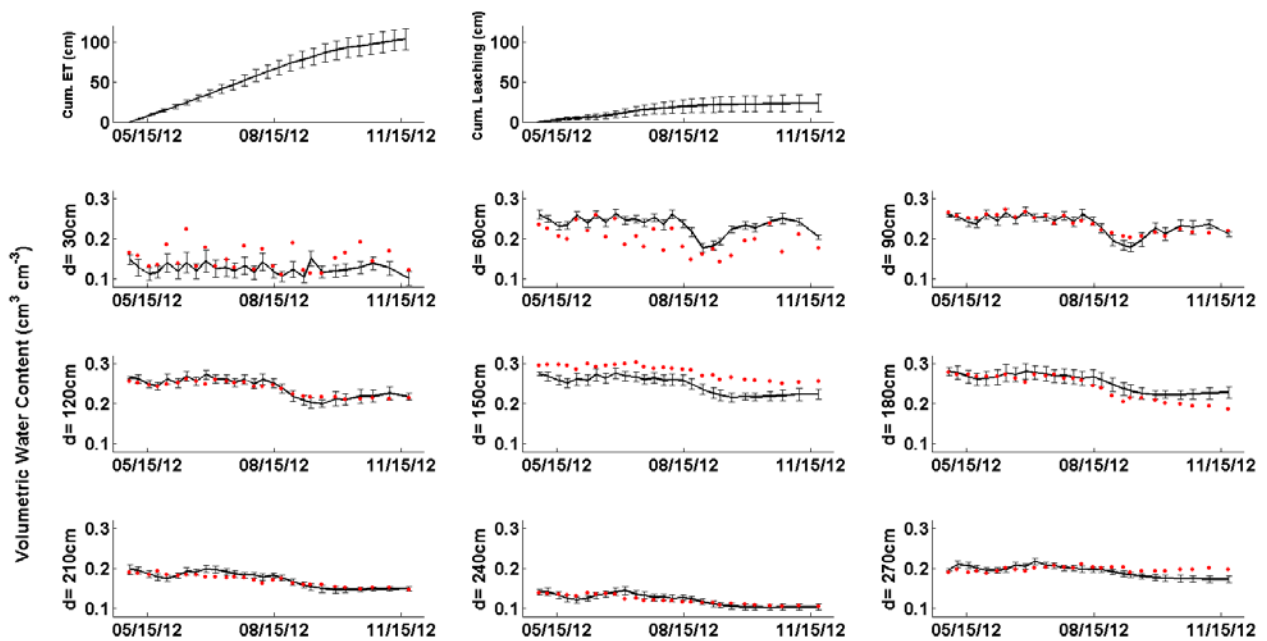


**Figure 14.** Simulated cumulative ET (top left), leaching (top middle), as well as observed (red circles) and simulated (black line) soil water content at nine different depths in fanjet tree (FT). The soil water content was measured by neutron probe at different depths (d) from 30 to 270 cm in 30 cm interval. Black lines show the average of simulated values in 16 different scenarios with error bars representing their variation defined by standard deviation.

**Figure 15** shows the average (thick black line) and standard deviation (error bars) of soil water retention and hydraulic conductivity curves predicted by inverse solution. It shows that the inverse modeling approach did not improve the uncertainty in hydraulic conductivity curves. The presented uncertainty in hydraulic conductivity curves is caused by (a) uncertainty in ET which was used as the top boundary condition in inverse modeling approach, and (b) the well-known non-uniqueness issue associated with using inverse modeling to predict unsaturated soil hydraulic properties. One way of reducing this uncertainty is to use both water content and soil matric potential as input data in the inverse modeling approach. We currently are conducting a series of inverse modeling scenarios to find a good fit for both water content and soil matric potential, thereby reducing the uncertainty in hydraulic conductivity curves which will be used to improve our estimated leaching using Darcy approach (section 4.3.2&3).

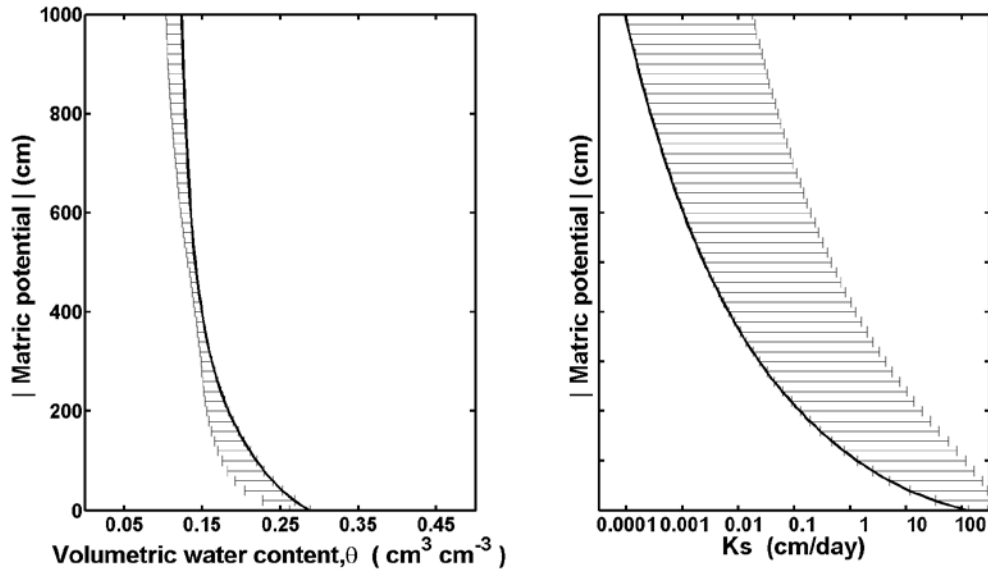


**Figure 15.** Soil water retention (left plots) and unsaturated hydraulic conductivity (right plots) curves predicted using inverse modeling approach for fanjet tree (FT). The error bars represent the standard deviation of 16 different curves.

#### 4.3.5. Estimation of local ET using artificial neural network (ANN) approach

The effect and importance of ET in estimating leaching in both the water balance and the modeling approach was evaluated and discussed in section 4.3.1 and 4.3.4. It was concluded that using field average ET introduces considerable amount of uncertainty in estimating leaching at local (tree plot) scale. In order to reduce this uncertainty one would need to use a downscaling approach to estimate ET at tree scale. Therefore, we used the artificial neural network (ANN) approach to downscale field actual evapotranspiration (ET<sub>a</sub>) to the individual tree scale ET<sub>a</sub>. The ANN calibrates a statistical relation between field ET<sub>a</sub>, tree midday stem water potential (MSWP), soil water storage (WS), and tree potential evapotranspiration (ET<sub>c</sub>) adjusted based on relative tree canopy cover (C<sub>rel</sub>). Hence, the ANN develops a functional relationship that explains transpiration rate adjustments to soil water limitation.

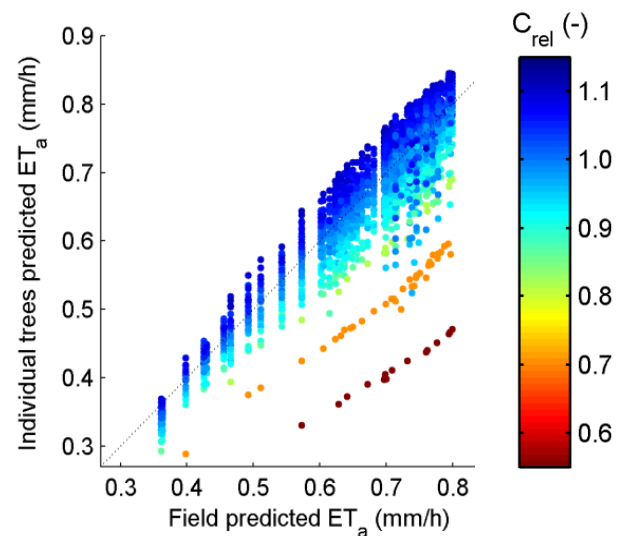


**Figure 16.** Comparison of field versus individual trees ET<sub>a</sub> predicted by the ANN. The color scale indicates the relative canopy cover (C<sub>rel</sub>) of individual trees.

Four years of field-average soil and almond trees water status data (collected on 40 trees, 75 times between April and September) were used to optimize the ANN to predict ET<sub>a</sub> values measured with the Eddy covariance tower. The best ANN had a root mean square error (RMSE) of 0.0246 mm/h and a determination coefficient (R<sup>2</sup>) of 0.944.

Assuming that individual trees respond to combinations of their MSWP, soil WS, and ETc in the same way as the average field would, the field scale optimized ANN is used to downscale ETa to the tree level. We concluded that relative canopy cover (Crel) was the main source of variability of tree ETa, while MSWP was the most controlling factor for the ratio of tree ETa to ETc (ETrel).

We also concluded that tree response to soil WS was largely controlled by effective root zone soil properties. Specifically, our analysis showed that tree response to soil water stress was different between the fanjet and drip-irrigated blocks because of soil textural differences and associated soil water retention properties.

In wet conditions, the predicted tree ETa followed a normal distribution (with relative standard deviation of about 5%), which was close to the Crel distribution. However, standard deviation values increased (7.6% for the whole orchard) during periods of water stress. Standard deviation values were smaller for the individual irrigation blocks, implying that a major source of ETa variability is caused by block differences in water stress response, as explained by different soil water retention properties between blocks. Under well-watered conditions, values of ETa in the drip block were 1.7% higher than the field-average. This difference increased to 4.4% when considering water stress periods only.

This information is being implemented into our modeling and water balance computation framework in order to reduce the uncertainty range at tree scale ET. Once it is fully implemented, we will use our updated framework to calculate the leaching of water below the root zone.

### **Research Effort Recent Publications:**

- Kandelous, M.M., Moradi, A. B., Couvreur, V., Baram, S., Hopmans, J. W. 2014. Monitoring and modeling of nitrate leaching in micro irrigation across a wide range of California crops and soils. Soil Science Society of America, Long Beach, CA.
- Kandelous, M.M., Sanden, B., Hopmans, J.W., 2013. A Unified Experimental Approach for Estimation of Root Zone Leaching of Applied Irrigation Water and Fertilizers. Soil Science Society of America, Tampa, FL.
- Kandelous, M.M., Olivos, A., Sanden, B., Brown, P., Hopmans, J.W., 2013. Optimization of Water Use and Nitrate Use for Almonds under Micro-Irrigation. Almond Board of California annual Meeting. Sacramento, CA.
- Kandelous, M.M., Moradi, A.B., Brown, P., Hopmans, J.W., 2013. Monitoring of water and nitrate leaching in an almond orchard, American Geophysical Union Fall Meeting, San Francisco, CA.
- Hopmans J.W., and Kandelous, M. M. 2013. How does Nitrogen move in the soil, and what are the factors that influence its movement. Citrograph, May/June 2013, pages 22-28.
- Kandelous, M.M., Moradi, A.B., Hopmans, J.W., Burger, M., 2012. coupled experimental-modeling approach for estimation of root zone leaching of applied irrigation water and fertilizers, AGU Fall Meeting. AGU, San Francisco.
- Kandelous, M.M, A. Olivos, P. Brown, and J.W. Hopmans, 2012. Optimization of water use and nitrate use for almonds under micro-irrigation. Almond Industry Conference, Sacramento, CA.

- Kandelous M.M., T. Kamai, J.A. Vrugt, J. Simunek, B.R. Hanson, and J.W. Hopmans. 2012. Evaluation of subsurface drip irrigation design and management parameters for alfalfa. *Agric. Water Management*. Doi:10.1016/j.agwat.2012.02.009.
- Kandelous, M.M, A. Olivos, P. Brown, and J.W. Hopmans, 2011. Optimization of water use and nitrate use for almonds under micro-irrigation. Almond Industry Conference, Modesto, CA.
- Hopmans, J.W., M.M. Kandelous, A. Olivos, B.R. Hanson and P. Brown. 2010. Optimization of water use and nitrate use for almonds under micro-irrigation. Almond Industry Conference, Modesto, CA.
- Kandelous, M.M, T. Kamai, J.A. Vrugt, J. Simunek, B.R. Hanson and J.W. Hopmans. 2010. An optimization model to design and manage subsurface drip irrigation system for alfalfa. AGU Fall meeting, San Francisco, CA.